# International Journal of MATERIALS RESEARCH Zeitschrift für METALLKUNDE Original Contributions

A. Kruk, G. Cempura: Application of analytical electron microscopy and FIB-SEM tomographic technique

# Adam Kruk, Grzegorz Cempura

AGH University of Science and Technology (AGH-UST), International Centre of Electron Microscopy for Materials Science and Faculty of Metals Engineering and Industrial Computer Science, Krakow, Poland

# Application of analytical electron microscopy and FIB-SEM tomographic technique for phase analysis in as-cast Allvac 718Plus superalloy

The superalloys are usually used as structural material in jet engines due to their high-temperature stability and good endurance. Many components found in the hot-part of jet engines are of complex shape, therefore casting is utilized for to their production. One of the problems associated with the casting process of highly alloyed alloys, such as superalloys, is partitioning of alloying elements upon solidification. This segregation might lead to the formation of low melting temperature eutectics. Their presence in the material microstructure will have a negative effect on the weldability. Negative impact on weldability is one of the reasons why secondary phases should be avoided as microstructural elements in the welded materials. To eliminate such hazardous phases, the material should be subjected to a heat treatment with the aim of homogenizing the microstructure and chemical composition, which should enhance the weldability. The aim of this work was the application of analytical electron microscopy in combination with energy dispersive X-ray spectroscopy as well as tomographic techniques for qualitative and quantitative characterization of structural elements in as-cast Allvac 718Plus Ni-based superalloy subjected to later heat treatment. Alloy 718Plus is a newly developed superalloy in which the secondary Laves phase forms as a low-melting eutectic upon casting. The development of innovative materials for aeronautics and clean energy systems requires the use of modern research methods for structure characterization on the level from micro- to the nanoscale. The performed analysis, allowed identification of phases (Laves and  $\eta$ ) occurring in interdendritic regions of as-cast Allvac 718Plus superalloy and analyzing their microstructure down to the atomic scale, which revealed their complex nature. The experiments and investigation show that advanced microscopic techniques and test methods in conjunction with tomographic techniques enable complementary information about solidified structures of the alloy to be obtained that can be useful for the understanding process of casting and welding of the Allvac 718Plus.

**Keywords:** ATI Allvac 718Plus; Laves phase; SEM-EDS; STEM-HAADF; FIB-SEM tomography

# 1. Introduction

The development of environmentally friendly energy systems requires the application of innovative materials and use of advanced techniques for characterization of their microstructure down to the nanoscale. Processing of alloy Allvac 718Plus (herein referred to as 718Plus), e.g., solidification, hot working and heat treatment practices, has to be carefully controlled to assure a desirable microstructure and therefore the required mechanical properties. 718Plus is a newly developed nickel-based superalloy characterized by good strength properties and corrosion resistance at ele-

vated temperature that has improved high-temperature performance compared to IN718 while retaining the excellent processing characteristics of IN718. To eliminate unstable  $\gamma''$  (Ni<sub>3</sub>Nb, D0<sub>22</sub> tetragonal) phase [1–4] and promote the formation of the more stable  $\gamma'$ -Ni<sub>3</sub>(Al,Ti), (L12 cubic, Pm3 m) phase [5–7], 718Plus has significant changes to the chemistry in comparison to IN718. The main differences are the addition of Co, lower Fe and a lower ratio of Ti to Al. Combination of different chemistry and heat treatment results in precipitation of  $\gamma'$ ,  $\delta$ ,  $\delta$  and  $\eta$  phases or  $\eta$  phase.

The microstructure of 718Plus consists of a  $\gamma$  (Ni-based solid solution) matrix with ordered fcc  $\gamma'$  type phase, some orthorhombic  $\delta$ -Ni $_3$ Nb (D0a, orthorhombic, Pmmn) and hexagonal  $\eta$ -Ni $_3$ Ti,  $\eta^*$ -Ni $_6$ AlNb or Ni $_6$ (Al,Ti)Nb, (Ni $_3$  · Nb $_{0.5}$ (Al/Ti) $_{0.5}$ , D0 $_{24}$ , hexagonal, P6 $_3$ /mmc) particles precipitated at the grain boundaries [8–12]. Nickel-based superalloys are used in jet engines due to their high-temperature stability and good endurance [13]. Morphology of  $\eta$ -phase precipitates in 718Plus depends on the thermo-mechanical treatment to which the alloy was subjected.

Often it occurs in colonies in a Blackburn orientation relationship  $\{111\}\gamma\parallel\{001\}\eta$  with one of the adjacent grains [8]. The  $\eta\text{-phase}$  precipitates grow in a disc-like morphology on the  $\{111\}\gamma$  a matrix plane towards the grain interior, the detailed mechanism has been suggested in [14]. It is also common to observe small fractions of fine  $\delta\text{-phase}$  sheets within  $\eta\text{-phase}$  discs [8, 14].

Components of aircraft engines and gas turbines have a complicated shape. Therefore casting is utilized for their production. One significant problem associated with the casting of highly alloyed alloys and nickel-based superalloys, is partitioning of elements upon solidification. As a result, this might lead to the formation of low melting temperature eutectics, which further will have an adverse effect on the weldability [15]. Segregation is a common problem in solidified structures such as castings and welds. It causes chemical inhomogeneity in the microstructure and hence is detrimental to the mechanical properties. Although both the castings and weld metal have solidified structures, they differ in mode of solidification, experienced thermal cycles, and level of segregation. Laves phase that forms in the interdendritic region as a result of segregation, is an important aspect of 718Plus welds because it affects structural integrity and can lead to premature failure of critical aircraft engine components during service [16– 18]. Therefore, any attempt to reduce the segregation of chemical elements in welds will be highly advantageous. The present work pursues this direction and the paper reports results of the application of analytical scanning- as well as transmission electron microscopy methods (SEM, TEM) and focused ion beam (FIB-SEM) tomographic technique for phase analysis in as-cast Allvac 718Plus superalloy. Primary attention was paid to the study of phases occurring in interdendritic areas.

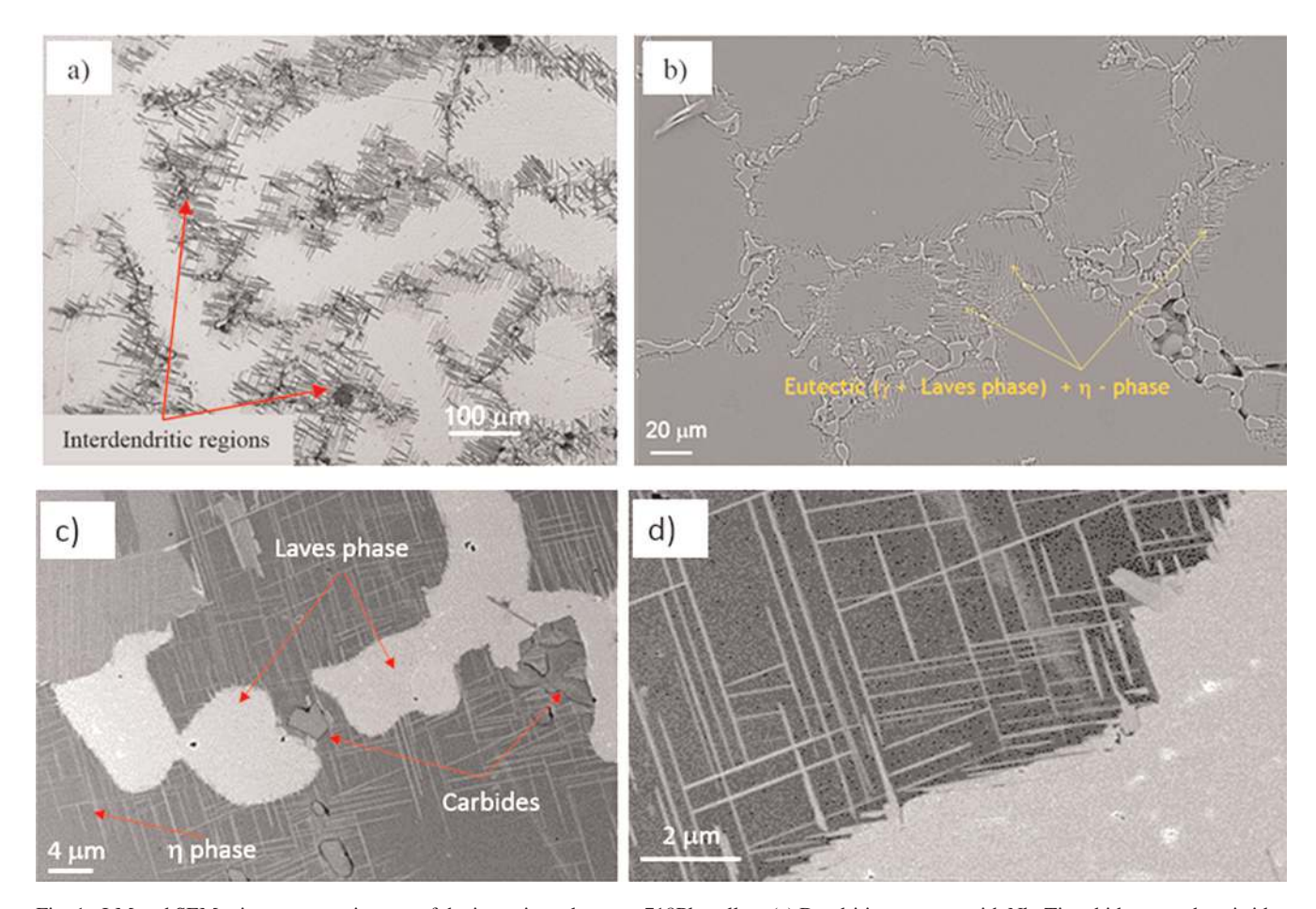


Fig. 1. LM and SEM microstructure images of the investigated as-cast 718Plus alloy. (a) Dendritic structure with Nb, Ti carbides or carbo-nitrides (MC +  $\gamma$ ), Laves ( $\gamma$  + Laves) eutectics and plate-like precipitates of  $\eta$ -phase in interdendritic regions, LM. (b, d) Different areas of the samples imaged at higher magnification, SEM.

# 2. Material and experiment

The present work focuses on the application of light microscopy (LM), SEM, TEM and FIB-SEM tomographic techniques for imaging and phase analysis in as-cast 718Plus superalloys subjected to heat treatment:  $1120\,^{\circ}\text{C/}4\,\text{h} + 968\,^{\circ}\text{C/}10\,\text{h}$ . The nominal chemical composition of 718Plus is the following: (wt.%): Ni - 8.72Co - 19.39Cr

– 0.04Ta – 1.04 W – 1.67Al – 8.79Fe – 0.867Ti – 2.76Mo – 6.10Nb – 0.01B. The SEM microstructural analysis was performed using a Merlin Gemini II scanning electron microscope. TEM and HRSTEM investigations were performed on an FEI Cs-corrected Titan G2 60-300 operating at 300 kV, equipped with energy dispersive X-Ray spectroscopy (EDX) ChemiSTEM technology. STEM imaging was performed in high angle annular dark-field (HAADF)

Table 1. The average concentration of chemical elements in different regions of as-cast 718Plus superalloy.

Average concentration and Standard deviation (at.%)	С	Ni	Cr	Fe	Со	Al	Nb	Mo	Ti	W
Dendrite arms/SEM-EDS	_	49.9	23.6	10.0	8.9	3.2	2.5	1.2	0.5	0.00
	_	0.02	0.33	0.57	0.26	0.06	0.85	0.10	0.19	_
Laves phase/SEM-EDS	_	38.2	18.3	6.8	10.2	0.8	21.6	3.6	0.4	0.00
	_	0.70	0.36	0.28	0.49	0.17	0.41	0.49	0.18	_
Laves phase/TEM-EDS	_	29.6	19.4	7.9	11.2	1.4	22.7	7.8	0.0	0.00
	_	0.07	0.06	0.33	0.51	0.34	0.95	0.54	0.02	-
γ phase between η plates	_	49.1	25.1	9.9	8.8	2.8	2.7	1.2	0.3	0.00
		1.22	0.64	0.59	1.43	0.66	0.69	0.36	0.18	_
Carbides/SEM-EDS	52.4	2.6	1.4	0.4	0.4	0.0	36.7	0.0	5.7	0.4
	0.41	1.05	0.61	0.29	0.19	_	1.59	_	0.41	0.07

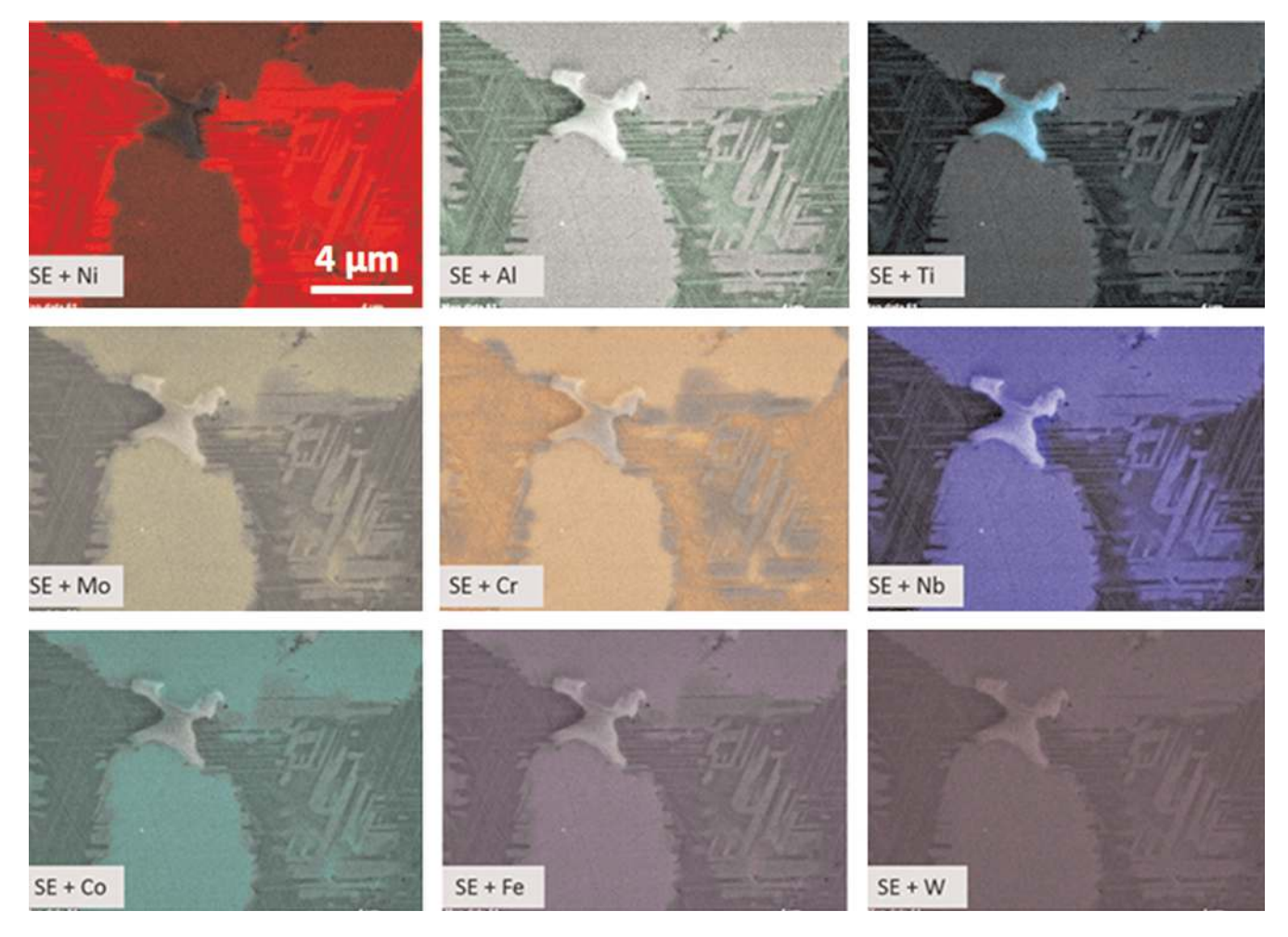


Fig. 2. SEM-EDS maps of selected chemical elements collected from interdendritic areas (Laves phase, carbide and plate-like precipitates η-phase) of as-cast 718Plus alloy.

mode. The TEM study was conducted on lamellae a prepared by FIB.

Analyses of the chemical composition of phases were performed using TEM-EDX and SEM-EDX methods. Analysis of crystallographic structure (phase composition) of selected particles was performed using the TEM selected area electron diffraction (SAED) method supported by JEMS software. 3D imaging of precipitates present in interdendritic regions was performed using FIB-SEM tomography. FIB NEON CrossBeam 40EsB with Ga-ion beam working at parameters: 30 kV, 1 nA was used to perform precise in-situ milling. Repeated removal of material layers as thin as 36 nm allowed exploration of a total volume of

 $10.5 \times 9.5 \times 5.9 \,\mu m$  ( $V = 588.5 \,\mu m^3$ ). The angle between the electron and the ion beams was  $54^{\circ}$  and mechanical movement of the specimen during milling was not necessary. The region of interest (ROI) of the sample's surface was selected by SEM-imaging. A protective layer of Pt was deposited over the area of investigation using the FIB-induced decomposition of precursor gases. This Pt layer serves not only as protection but helps in suppressing curtaining effects improving the quality of the surface milling. To improve the phase identification and their 3D reconstruction, a backscattered electron (BSE) detector, which offers an alternative contrast (Z-contrast) mechanism, was used. As a result, the acquired stack of images (image size

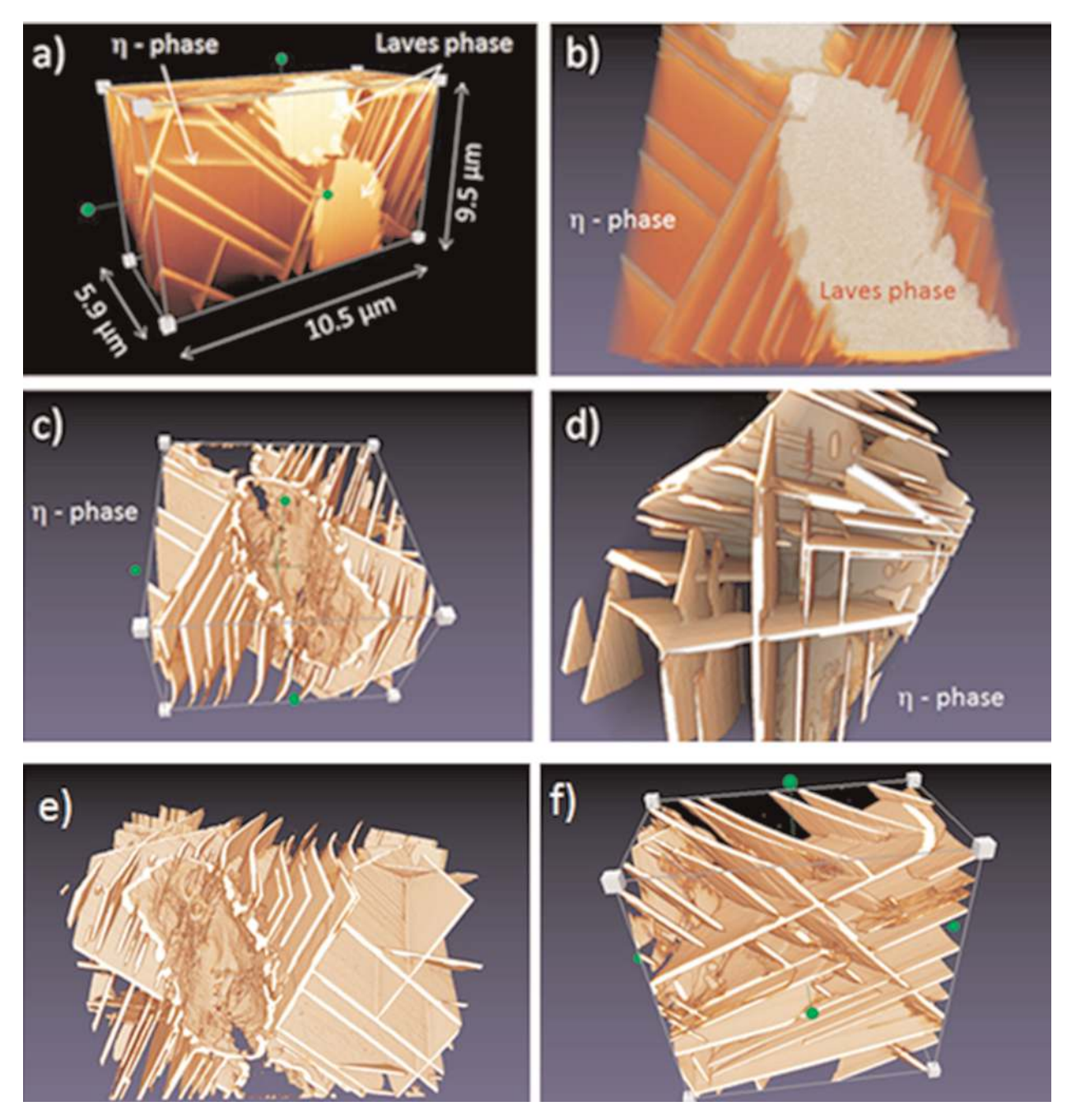


Fig. 3. Result of tomographic reconstruction (3D visualization) of a Laves phase with  $\eta$ -phase as platelet shaped particles; a) visualization of reconstructed volume  $10.5 \times 9.5 \times 5.9$  µm, (b) Laves phase with  $\eta$ -phase plate particles which precipitation starts at the interface of the Laves phase, (c) 3D visualization of a Laves phase with  $\eta$ -phase rendered from reconstructed volume, (d) 3D visualization of plate-like  $\eta$ -phase precipitates, (e, f) visualization in 3D reconstructed volume at different angles of view.

 $1024 \times 768$  pixels, 378 images in 8-bit grayscale, stack size 147 MB) was transformed directly into a 3D data volume with a voxel size of  $18 \times 18 \times 36$  nm. The shift between consecutively recorded images in the lateral direction due to slice cutting and/or electrical and mechanical instability of the device during recording of the tomogram (a series of images) was calculated and subsequently corrected with ImageJ 1.45b software. Based on the set of SEM micrographs, the 3D reconstruction and visualization of the investigated alloy volume were created using ImageJ 1.45b and Avizo Fire 6.3 software.

### 3. Results and discussion

Based on LM and SEM analysis, the microstructure of investigated as-cast 718Plus alloy consists of dendritic structure with interdendritic regions decorated with a continuous network of a structure with darker contrast (Fig. 1a): Nb-Ti carbide or carbo-nitride ( $MC + \gamma$ ), Laves ( $\gamma + \text{Laves}$ ) eutectics and plate-like precipitates of  $\eta$ -phase (Ni<sub>3</sub>Ti D0<sub>24</sub>) presents in interdendritic regions. From a morphological point

of view, the carbides have very complex forms, often called "Chinese scripts". The microstructure of the specimen observed with LM and SEM is presented in Fig. 1: needle-like  $\eta$ -phase irregular in shape of Laves phase particles (Fig. 1a and d) and randomly distributed niobium rich MC-type primary carbides (36.7Nb – 5.7Ti and 52.4C in at.%, see Table 1), (Fig. 1c).

After casting, alloy 718Plus is heavily segregated. Two areas with different chemical composition were identified: the dendrites that are very high in Fe, Cr, and Ni, whose concentrations in at.% is respectively equal to 10, 23.6, and 49.9 (Table 1) while the interdendritic areas are enriched in Nb, Mo, and Ti. EDS microanalysis shows strong segregation of Nb: a "dendritic" Nb content is as low as 2.5 at.% while Nb levels in the interdendritic regions can range as high as 12%.

The average chemical compositions of selected phases present in the interdendritic region determined using SEM-EDS and TEM-EDS methods are presented in Table 1. The Laves phase appears as islands, contains about 22 at.% Nb and forms preferentially in the interdendritic

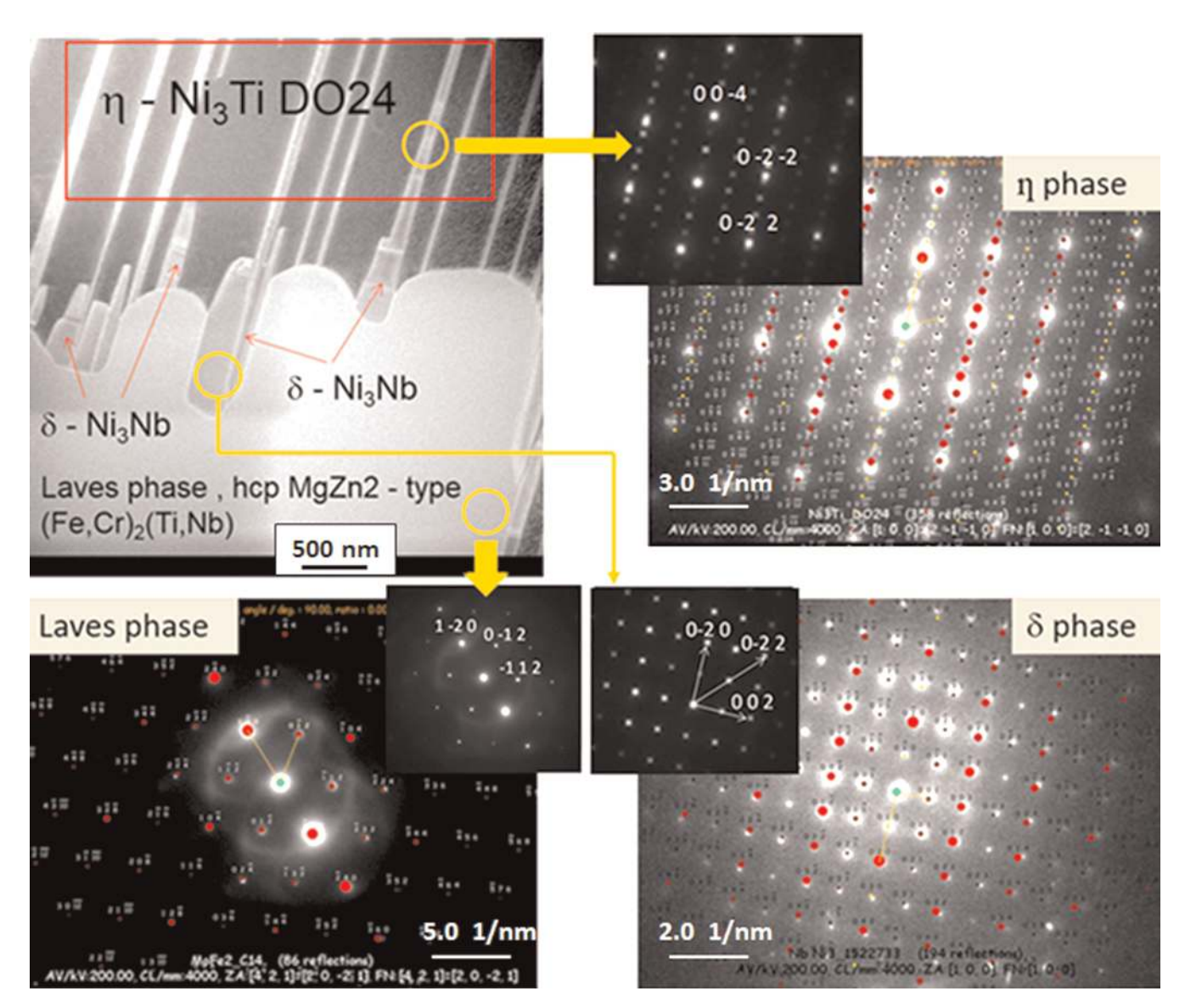


Fig. 4. TEM-SAED analysis of phases observed in lamellae prepared from as-cast 718Plus alloy using FIB technique.

areas where high Nb level existed. The formation of Laves phase is promoted by the presence of Mo and Si [19]. Since the Laves phase is detrimental to mechanical properties and depletes the matrix of Nb, the conditions of thermal treatments during homogenization are critical [19]. Islands of Laves phase can be crack initiation sites. Therefore, LCF (low cycle fatigue) life is impaired when Laves phase is present [20]. The Nb segregation during ingot or casting solidification is related to the rate of cooling and the ease with which the atoms can diffuse, i. e., the faster the cool, the less the segregation. During solidification, the  $\gamma$  matrix rejects the large atoms selectively of elements such as Nb, Mo, Ti to the interdendritic regions. These elements form NbC, TiN, and the Nb-rich Laves phase in the Nb enriched areas.

Annealing at  $1120\,^{\circ}\text{C/4}\,\text{h} + 968\,^{\circ}\text{C/10}\,\text{h}$  does not cause Laves phase to disappear but leds to the precipitation of the plate-like  $\eta$  phase precipitates near interdendritic areas, where the Nb content is still high. The primary MC and the TiN phases in alloy 718Plus are considered to be stable phases and will not change with thermal cycles at lower temperatures. The chemical composition of the area between the plate-like  $\eta$  phase precipitates corresponds to the chemical composition of the dendrite arms.

SEM-EDS maps of selected chemical elements collected from interdendritic areas of as-cast 718Plus alloy suggest phases such as Laves phase, carbide and plate-like precipitates  $\eta$ -phase (Fig. 2). Based on the results of chemical composition, it can be concluded that chemical elements

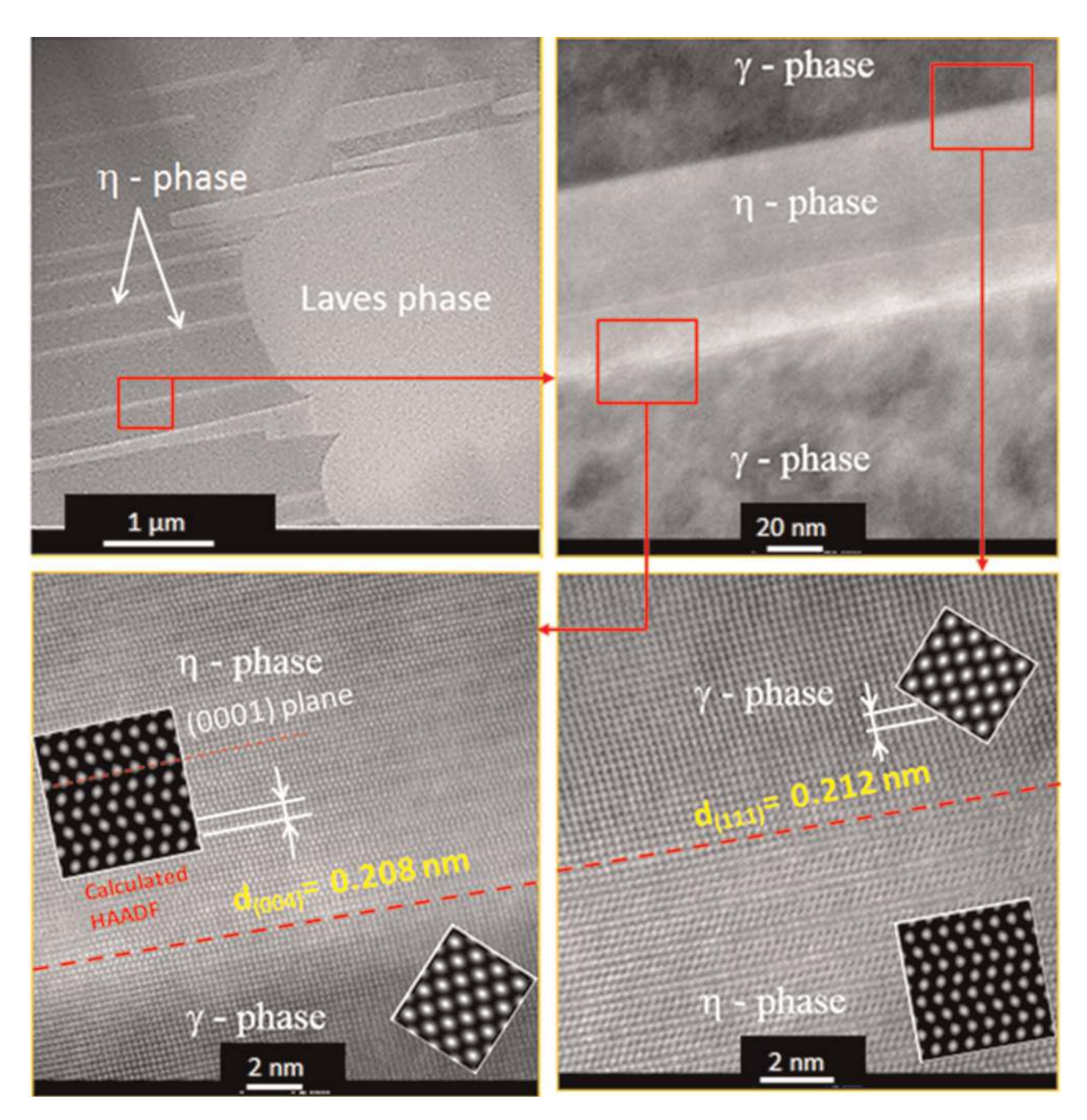


Fig. 5. HRSTEM-HAADF imaging of plate-like particle  $\eta$  phase. High-resolution imaging of the  $\eta/\gamma$  interface with theoretical HAADF images for the corresponding  $(\eta, \gamma)$  phases.

such as Ni, Mo, Cr, Nb, Co, Fe, and W take part in the formation of Laves phase precipitates. Plate-like precipitates of η-phase contain mainly Nb, Al and Ni. The carbide particle visible in Fig. 2 is mainly composed of Nb and Ti. It is worth emphasizing that on the Al map, there are also noticeable plate-shaped precipitates in which there is no Al, they contain Nb and Ni. Based on these results, they can be identified as plate-like precipitates of  $\delta$ -phase (Ni<sub>3</sub>Nb). The Ni elemental map shows the significant enrichment in this element of the outer layer of the Laves phase. This area is also depleted in the remaining non-Nb elements (Fig. 2). The precipitates of the carbide phase, which are shown in Fig. 2 between the Laves phase particles, are mainly composed of Nb and Ti, which was confirmed by the results of the SEM-EDS analysis presented in Table 1. They are most probably MC-type primary carbides where M is Nb + Ti. Result of X-ray diffraction (XRD) analyses, not presented in this paper, confirmed the presence of Nb<sub>4</sub>C<sub>3</sub> or Nb<sub>6</sub>C<sub>5</sub> type carbides in the investigated alloy.

Meso-scale FIB-SEM tomography was used for visualization and characterization of the interdendritic regions, mainly Laves phase and  $\eta$  phase precipitates, in as-cast 718Plus superalloy. The registered contrast level between  $\eta$ -phase and Laves phase (as seen by the energy selective backscattered, EsB, detector) allows us to perform a tomographic reconstruction of microstructural elements using the FIB-SEM tomography technique. The choice of optimal place for tomographic reconstruction depends on the contrast level between structural elements present in the microstructure during SEM-BSE observation. The difference in contrast level between areas with different crystallographic orientation is a result of the channeling effect. The apparent differences in image contrast between  $\eta$  and Laves phase particles and  $\gamma$ matrix enabled tomographic reconstruction of these phases, presented on Fig. 3a. Visualization of a Laves phase single particle with plates of  $\eta$ -phase growing out of its surface is presented in Fig. 3. A more detailed analysis of the tomographic reconstruction results shows that the precipitation of the  $\eta$ -phase platelets begins in the outer surface of the Laves phase. It starts in areas where the elevated concentration of Ni atom is observed (Ni elemental map in Fig. 2).

Figure 4 shows an image of the Laves phase particle observed in STEM-HAADF mode. The thin plate-like particles of  $\eta$ -phase nucleate from the outer surface of Laves phase particle. The contrast intensity of STEM-HAADF images is closely related to the atomic number Z, being approximately proportional to  $Z^2$ , and is partially mixed with the diffraction contrast. The intensity of the Laves and  $\eta$ -phases is brighter, because they contain chemical elements (e. g. Nb) with higher mean atomic number than  $\gamma$  matrix.

The selected area electron diffraction (SAED) patterns from the irregularly shaped bright particle visible in Fig. 4 revealed that this particle is a Laves phase (Fe,Cr,Ni)<sub>2</sub>(Nb, Mo,Ti), (hcp, MgZn<sub>2</sub>-type), while thin plate-like particles are the  $\eta$ -phase. The hexagonal crystal structure of the lamellar phase indicated  $\eta$ -Ni<sub>3</sub>Ti D0<sub>24</sub> phase, but its chemistry was close to Ni<sub>6</sub>(AlTi)Nb (see Ref. [8]). Pickering et al. [8] reported discontinuous precipitation of Ni<sub>6</sub>(Al,Ti)Nb phase. It should be emphasized that the thicker and shorter plates that grow directly from the Laves' surface areas as observed in Fig. 4, are plates of  $\delta$ -phase (Ni<sub>3</sub>Nb), which was confirmed by the SAED analysis (see Fig. 4). Analysis of diffraction patterns was supported by the JEMS ver. 3.69

software. Results of HRSTEM-HAADF imaging and analysis of plate-like particle  $\eta$ -phase precipitate in  $\gamma$  matrix are presented in Fig. 5. High-resolution imaging of the  $\eta/\gamma$  interface with theoretical HAADF images for the corresponding  $(\eta, \gamma)$  phases are also included. Selected area electron diffraction patterns (SAED) and HAADF image analysis allowed defining mutual crystallographic relations between  $\gamma/\eta$  phases. The precipitate  $\eta$ -phase and  $\gamma$  matrix were found to be related through the Blackburn orientation relationship:  $(11\bar{1})\gamma \parallel (000\bar{1})\eta$  and  $[0\bar{1}\bar{1}]\gamma \parallel [\bar{2}110]\eta$ .

### 4. Conclusions

Based on the results of these studies, it can be stated that interdendritic areas of as-cast 718Plus nickel-based superalloy subjected heat treatment  $1120\,^{\circ}\text{C/4}\ h + 968\,^{\circ}\text{C/10}\ h$  consist of eutectics which are composed of MC type carbides, Laves phase and plate-like precipitates of  $\eta$ -phase.

Based on the chemical composition results, it can be concluded that chemical elements such as Ni, Mo, Cr, Nb, Co, Fe, and W take part in the creation of Laves phase precipitates. The TEM-SAED diffraction analysis showed that Laves phase precipitates are a hexagonal MgZn<sub>2</sub> type phase with a chemical composition similar to (Fe, Cr, and Ni)<sub>2</sub>(Nb, Mo, and Ti).

Plate-like precipitates of  $\eta$ -phase contained mainly Nb, Al, and Ni and precipitated on the {111} type plane of the  $\gamma$  matrix. Plate-shaped precipitates were identified as Ni<sub>3</sub>Ti D024 with a chemical composition similar to Ni<sub>6</sub>(AlTi)Nb.

The results of 3D imaging performed using the FIB-SEM tomographic technique indicate that the precipitation of lamellar  $\eta$ -phase starts from the outer surface of the Laves phase.

The authors acknowledge the support from the AGH-UST statutory project (nr. 11.11.110. 299).

### References

- [1] D.F. Paulonis, J.M. Oblak, D.S. Duvall: Trans ASM 62 (1969) 611.
- [2] I. Kirman, D.H. Warrington: J. Iron Steel Inst. 205 (1967) 1264.
- [3] R.L. Kennedy: Superalloys 718, 625, 706 and Derivatives (2005) TMS 1.
- [4] W. Cao, R. Kennedy: Superalloys (2004) TMS.
- [5] R.L. Kenney, W.D. Cao, T.D. Bayha, R. Jeniski, Niobium, High Temperature Applications (2003) TMS 11.
- [6] W.D. Cao, US patent 6730.254 B2 (2004).
- [7] W.D. Cao, Kennedy RL: Superalloys (2004) TMS 91.
- [8] E.J. Pickering, H. Mathur, A. Bhowmik, O.M.D.M. Messé, J.S. Barnard, M.C. Hardy, R. Krakow, K. Loehnert, H.J. Stone, C.M.F. Rae: Acta Mater. 60 (2012) 2757. DOI:10.1016/j.actamat.2012.01.042
- [9] L. Viskari, Y. Cao, M. Norell, G. Sjóberg, K. Stiller: Mater. Sci. Eng. A 528 (2011) 2570. DOI:10.1016/j.msea.2010.11.080
- [10] L. Viskari, K. Stille: Ultramicroscopy 111 (2011) 652. PMid:21295914; DOI:10.1016/j.ultramic.2011.01.015
- [11] C. Stotter, C. Sommitsch, J. Wagner, H. Leitner, I. Letofsky-Papst, G.A. Zickler, W. Prantl, M. Stockinger: Int. J. Mater. Res. 99 (2008) 376. DOI:10.3139/146
- [12] R. Krakow, D.N. Johnstone, A.S. Eggeman, D. Hünert, M.C. Hardy, C.M.F.Rae, P.A.Midgley: Acta Mater. 130 (2017) 271. DOI:10.1016/j.actamat.2017.03.038
- [13] X. Xie, G. Wang, J. Dong, C. Xu, W.D. Cao, R.L. Kennedy: All-vac® 718plus<sup>TM</sup>Superalloys, 718 and Derivatives (2005) Warrendale, PA: TMS 179.
- [14] O.M. Messé, J.S. Barnard, E.J. Pickering, P.A. Midgley, C.M.F. Rae: Philosophical Magazine 94 (2014). DOI:10.1080/14786435.2013.878052

- [15] K.R. Vishwakarma, N.L. Richards, M.C. Chaturvedi: Superalloys 718, 625, 706 and Derivatives (2005) TMS.
- [16] G.K. Bouse: Superalloy 718 Metallurgy and Applications (1989) TMS 69.
- [17] M.J. Ceislak, G.A. Knorovsky, T.J. Headley, A.D. Romig, Jr: Superalloy 718 (1989), 59 TMS-AIMS, Warrendale, 59.
- [18] W.D. Cao: Superalloys 718, 625, 706 and Derivatives (2005) TMS.
- [19] J.F. Radavich: Superalloy 718-Metallurgy and Applications (1989) TMS 229.
- [20] J.J. Schirra, R.H. Caless, R.W. Hatala: Superalloys 718, 625 and Various Derivatives (1991) TMS.

(Received November 29, 2017; accepted April 5, 2018; online since July 16, 2018)

### Correspondence address

Professor Adam Kruk AGH University of Science and Technology Al. Mickiewicza 30, Kraków 30-059 Poland

Tel.: +48 12 617 2566 E-mail: kruczek@agh.edu.pl Web: www.tem.agh.edu.pl

## **Bibliography**

DOI 10.3139/146.111678 Int. J. Mater. Res. (formerly Z. Metallkd.) 110 (2019) 1; page 3–10 © Carl Hanser Verlag GmbH & Co. KG ISSN 1862-5282